

Enhancing spontaneous emission rates of molecules using nanopatterned multilayer hyperbolic metamaterials

Dylan Lu¹, Jimmy J. Kan², Eric E. Fullerton^{1,2} and Zhaowei Liu^{1,2,3*}

Plasmonic nanostructures have been extensively used to manipulate the spontaneous light emission rate of molecules and their radiative efficiency^{1–6}. Because molecules near a metallic surface experience a different environment than in free space, their spontaneous radiative emission rate is generally enhanced^{7–9}. Such enhancement, measured by means of the Purcell factor, arises as a consequence of the overlap between the surface plasmon mode frequency and the emission spectrum of the molecule. However, such overlap is available only for a few narrow bands of frequency due to the limited plasmonic materials existing in nature^{10,11}. Although this limitation can be overcome by using hyperbolic metamaterials (HMMs)—a type of nanoscale artificial material with hyperbolic dispersion relations—the Purcell factor and the radiative power have remained relatively low^{12–16}. Here, we show that by nanopatterning a hyperbolic metamaterial made of Ag and Si multilayers, the spontaneous emission rate of rhodamine dye molecules is enhanced 76-fold at tunable frequencies and the emission intensity of the dye increases by ~80-fold compared with the same hyperbolic metamaterial without nanostructuring. We explain these results using a dynamic Lorentzian model in the time domain.

Metamaterials offer new routes to the design of materials with attractive optical properties for potential applications in super-resolution imaging and multifunctional devices^{17–19}. Metamaterials composed of a stack of multilayers are particularly promising because of their unique, hyperbolic dispersion relation^{20–24}. When brought into the near-field of multilayer metamaterials, light emitters release their energy predominantly via three channels: radiative emission, plasmonic modes and other non-radiative decay modes^{10,11}. Plasmonic modes usually dominate over other decay channels^{20,21}. Because of their tunable dispersion relations, HMMs offer a larger plasmonic density of states (DOS) at any desired wavelength, which leads to an enhancement in spontaneous emission rates. However, the difficulties in fabricating metal–dielectric multilayer HMMs at deep subwavelength scales, as well as the non-radiative nature of the dominating plasmonic modes in uniform HMMs, limit Purcell enhancement and the external quantum efficiency in the far-field. Accordingly, an outcoupling mechanism is necessary to extract energy from the non-radiative plasmonic modes.

Figure 1a presents the schematic configuration of the proposed HMM structure, which consists of nanopatterned Ag–Si multilayers. This multilayer combination was selected based on the optical properties and the compatibility of film growth (see Methods for more details). A scanning electron microscope (SEM) image of one of the fabricated samples is shown in Fig. 1b. The individual

Si and Ag layers are not visible due to the limited resolution in this SEM image. Dark-field scanning transmission electron microscope (STEM) images of the cross-sectional view at different magnifications indicate a well-formed periodic lattice structure in the Ag–Si multilayers with a highly conformal coating across the substrate (Fig. 1c). There is no accumulation of film roughness along the growth direction, and 10 nm layer thicknesses are consistently achieved. The element mapping for Si and Ag verifies the multilayer structure and some minor diffusion of Ag into Si (Fig. 1d). The layer thicknesses and multilayer structure were also confirmed by X-ray reflectivity scans.

We first calculated the Purcell factor⁷ based on a modified theory of dipole interaction with metal films to characterize the plasmonic DOS of the multilayer system (Supplementary Section 1). Figure 2a,b shows the normalized dissipated power spectra for perpendicular dipoles at a distance of $d = 10$ nm above the Ag film and the Ag–Si multilayer HMM, respectively, at various emission wavelengths. These graphs present the k -space power distribution of the spontaneous emission and indicate the presence of different decay channels. Components with a wavenumber less than $\sqrt{\epsilon_1}k_0$ correspond to power propagating in the surrounding dielectric medium with permittivity ϵ_1 , whereas those larger than $\sqrt{\epsilon_1}k_0$ are dominated by non-radiative parts, including plasmonic modes, where k_0 is the magnitude of the wavevector in vacuum.

By integrating normalized dissipated power across all wavenumbers, the resulting Purcell factor quantifies the spontaneous emission-rate enhancement at different emission wavelengths (Fig. 2c,d). The Purcell factor for a bulk Ag layer peaks at $\lambda = 360$ nm with a narrow bandwidth of ~10 nm (Fig. 2c), corresponding to surface plasmon resonance of the Ag film. In contrast, for the Ag–Si multilayer HMM the Purcell factor peaks around $\lambda = 600$ nm with a much broader bandwidth of over 60 nm (Fig. 2d), which aligns better with the emission spectrum of Rhodamine 6G (R6G). The Purcell enhancement at 600 nm is ~60-fold on the Ag–Si multilayer HMMs but less than tenfold on the Ag film. By adjusting the filling ratio of Ag in HMMs, the Purcell enhancement can be tuned, as shown in Fig. 2e, demonstrating the versatility of plasmonic DOS engineering in multilayer HMMs to achieve better control of emission processes at desired wavelengths. Three-dimensional full-wave simulation results (Supplementary Section 2) agree well with the theoretical calculations (provided as open circles in Fig. 2c,d).

We used the full-wave simulation method to study the interaction of dipole emitters with the nanopatterned multilayer HMM. Figure 3a,b presents the calculated cross-sectional mapping of the Purcell factor and the enhancement of radiative

¹Department of Electrical and Computer Engineering, University of California, San Diego, 9500 Gilman Drive, La Jolla, California 92093-0407, USA, ²Center for Magnetic Recording Research, University of California, San Diego, 9500 Gilman Drive, La Jolla, California 92093-0401, USA, ³Materials Science and Engineering, University of California, San Diego, 9500 Gilman Drive, La Jolla, California 92093-0418, USA. *e-mail: zhaowei@ucsd.edu

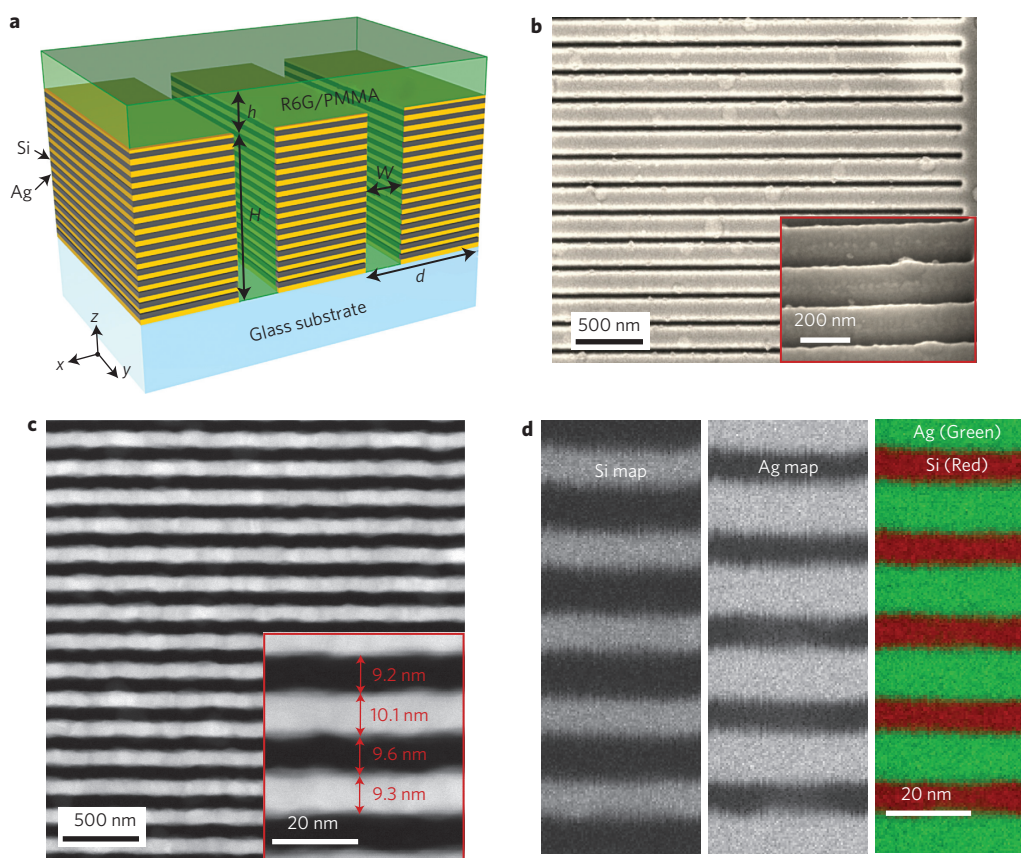


Figure 1 | Nanopatterned multilayer HMMs. **a**, Schematic configuration of nanopatterned multilayer HMMs on a glass substrate. The multilayers consist of Ag-Si stacks (thickness of each layer, 10 nm; total thickness H , 305 nm). Grating patterns with different periods are formed in the multilayers by FIB milling. The R6G dye molecules mixed in PMMA are spin-coated onto the surface to a thickness of $h = 80$ nm. **b**, SEM image of one of the fabricated nanopatterned HMMs (period $a = 200$ nm; width $w = 40$ nm). Inset: tilted-angle SEM image of the grating nanostructure. **c**, Dark-field STEM images of the cross-sections of Ag-Si multilayers under different magnifications, showing well-formed periodic lattice structures (each layer thickness, ~ 10 nm). The white colour corresponds to Ag and the black to Si. **d**, Element mapping for the constituent materials (Si and Ag), verifying the established multilayer lattice with some minor diffusion of Ag into Si.

emission for isotropic dipole emitters placed at different locations on uniform and nanopatterned Ag-Si HMMs at $\lambda = 600$ nm. Data corresponding to the dashed lines are replotted in Fig. 3c,d for a direct comparison of the characteristics on different substrates. The Purcell enhancement for a uniform HMM is known to decay exponentially away from the substrate, that is, along the z -axis. The introduction of nanopatterning in uniform HMMs leads to new variations in the Purcell factor in the x - y plane. The nanopatterned HMM retains a similar trend in Purcell enhancement at x - y locations away from the nanoslit, but has weak enhancement close to the nanoslit opening due to effectively larger emitter-metamaterial distances. At dipole locations 1, 2 and 3 (Fig. 3a), the Purcell factor as a function of emission wavelength (Fig. 3e) further illustrates the local plasmonic DOS and the spectral similarity between uniform and nanopatterned multilayer HMMs, whereas the Purcell enhancement close to the sidewall of the nanoslit shifts to longer wavelengths because of the anisotropic material property of the multilayer HMMs.

Thanks to the outcoupling effect of the grating, radiative emission is significantly enhanced on nanopatterned multilayer HMMs compared with uniform ones, as shown in Fig. 3b (for calculation details see Supplementary Section 2). The radiative emission on the uniform HMM is almost invariant with emitter-metamaterial distance, whereas on the nanopatterned multilayer HMM it has strong enhancement close to the surface of the HMMs where higher plasmonic DOS is available for outcoupling

(see the mapping of the Purcell factor in Fig. 3a). The corresponding spectra of radiative enhancement for dipole locations 1', 2' and 3' (Fig. 3b) are also shown in Fig. 3f. In comparison with the uniform HMM, radiative emission on the nanopatterned HMM is improved by over 100% at the peak wavelength, which will lead to the same improvement in the external quantum efficiency of dipole emitters (Supplementary Fig. 1). It is worth noting that the radiative enhancement factor relies on the geometry of the nanopatterns (see also Fig. 5).

To identify, experimentally, the Purcell enhancement of the multilayer HMMs, the lifetime of R6G dye molecules on various samples was measured and compared by time-resolved photoluminescence in a two-photon microscope system (see Methods). Figure 4 shows the measured time-resolved fluorescence decay curves (open circles), with peaks normalized to unity, for R6G on both nanopatterned Ag-Si HMM (Fig. 4,iv) and Ag grating (Fig. 4,ii) substrates. The lifetime of R6G in methanol solution (as a reference) was determined to be 3.8 ns according to the corresponding decay curve (black circles), which agrees well with the typical value in the literature²⁵. Unlike the case of R6G in methanol, the decay rate for the nanopatterned Ag-Si HMM and the Ag grating cannot be fit by a single-exponential function, because the detected fluorescence signals arise from the collective responses of the molecules randomly distributed in polymethyl methacrylate (PMMA) (Fig. 1a). For the nanopatterned Ag-Si HMM sample with a period of 200 nm, the fluorescence intensity initially decays

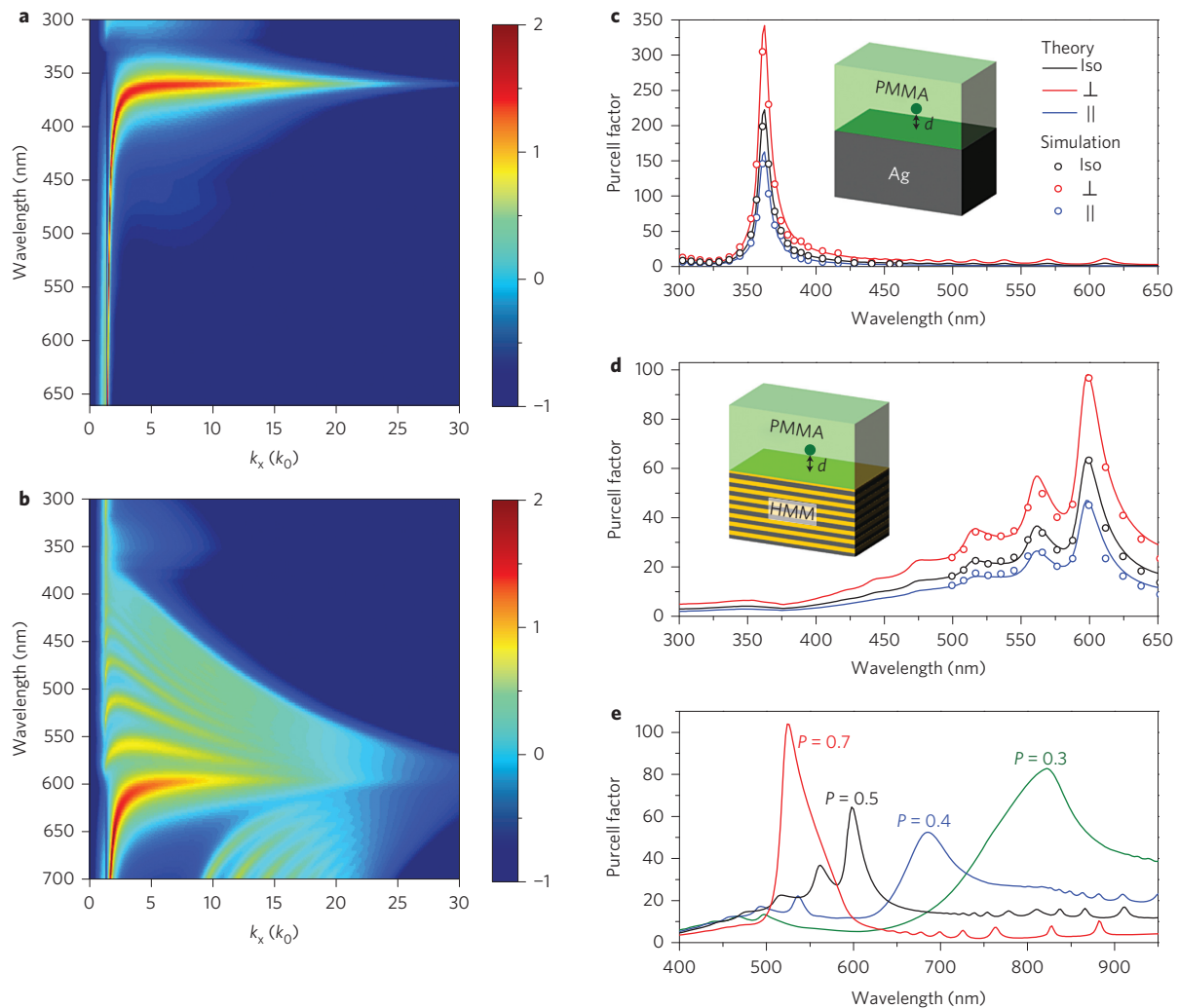


Figure 2 | Comparison of Purcell factors for Ag-Si multilayer HMMs and a pure Ag single layer. **a, b**, Normalized dissipated power spectra (intensity on a logarithmic scale) for a dipole perpendicular to and at a distance of $d = 10$ nm above a uniform Ag single layer (**a**) and a Ag-Si multilayer HMM (**b**), each with the same total thickness of 305 nm. The multilayer has 15 pairs of Ag and Si layers (each layer thickness, 10 nm). The colour scales indicate normalized dissipated power. **c, d**, Purcell factor for a dipole located $d = 10$ nm above the uniform Ag single layer (**c**) and the Ag-Si multilayer HMM (**d**), as depicted in the insets. The Purcell factor for isotropic dipoles (iso, black lines) is averaged from that for the dipoles perpendicular (\perp , red lines) and parallel (\parallel , blue lines) to the surface. Corresponding three-dimensional full-wave simulations (open circles) agree with theoretical calculations. **e**, Tunable Purcell enhancement across the visible spectra for isotropic dipoles located $d = 10$ nm above the uniform Ag-Si HMMs by adjusting the volumetric filling ratio of the metal, P .

at a maximum rate of $\sim 1/(0.070 \pm 0.003) \text{ ns}^{-1}$ which is attributed to the molecules strongly coupled to the HMM structure, before slowing to a minimum rate of $1/(2.2 \pm 0.3) \text{ ns}^{-1}$, which is determined mainly by those molecules away from the HMM. By the same token, for the Ag grating sample, the decay rates at the maximum and minimum are $1/(0.40 \pm 0.03) \text{ ns}^{-1}$ and $1/(2.0 \pm 0.1) \text{ ns}^{-1}$, respectively (Supplementary Fig. 2). The HMMs with plasmonic DOS aligned with the molecular emission spectra further enhance the decay rate by about one order of magnitude compared with the pure Ag gratings. A total 54-fold Purcell enhancement of the decay rate was measured for R6G on the nanopatterned HMM with a period of 200 nm at the emission wavelength (Supplementary Fig. 3 shows a comparison with pure Si films).

Figure 4 also shows the results for the uniform Ag-Si HMM (Fig. 4,iii) and the Ag single layer (Fig. 4,i) after division by the same normalization factor as used for the nanopatterned Ag-Si HMM and Ag grating, respectively. Compared with uniform films, a stronger Purcell enhancement was detected in both the nanopatterned HMM and the Ag grating. The grating nanostructures outcouple the dominating plasmonic modes in the HMM

for better far-field detection of fast-decaying signals from molecules strongly coupled to the metamaterials. Not only does the strong Purcell effect become accessible in the far-field—the fluorescence intensity is also enhanced significantly.

A systematic study of the geometrical dependence of decay rate and intensity enhancement was carried out for nanopatterned HMMs with different grating periods. Figure 5a shows that the measured lifetime of R6G further decreases as the period of the grating reduces. A correspondingly larger Purcell factor results in a total 76-fold decay-rate enhancement for R6G on the nanopatterned HMM with a period of 80 nm. The fluorescence intensity image accumulated over 100 frames at the emission wavelength was also captured on the area with both nanopatterned and uniform Ag-Si HMM regions. The ratio of the averaged intensity for the nanopatterned region and the uniform region identifies the fluorescence intensity enhancement (Supplementary Fig. 4). As shown in Fig. 5b, an enhancement factor close to 80-fold was achieved for the nanopatterned HMM with a period of 80 nm, compared with an eightfold intensity enhancement for larger periods. This intensity enhancement on nanopatterned HMMs results

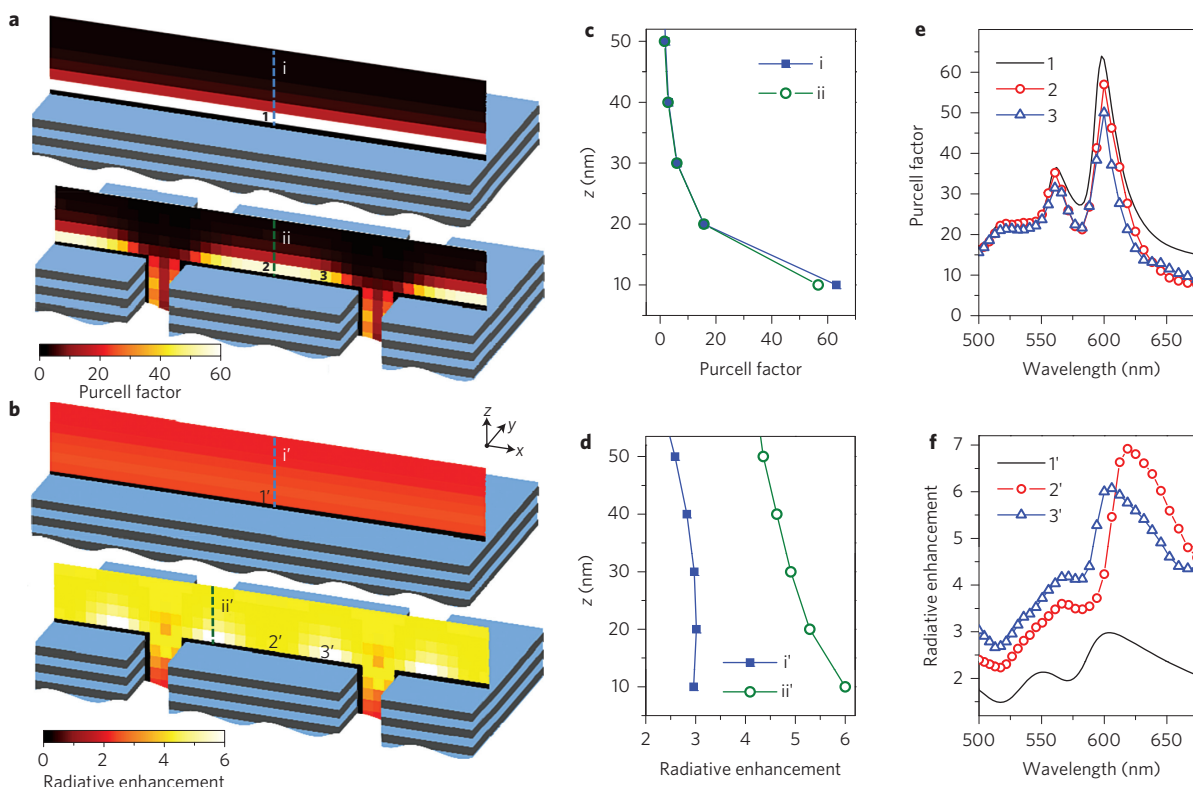


Figure 3 | Comparison of Purcell enhancement for uniform and nanopatterned multilayer HMMs. **a,b**, Cross-sectional mapping of Purcell factor (**a**) and radiative enhancement (**b**) for isotropic dipoles on the uniform and nanopatterned multilayer HMMs at an emission wavelength of 600 nm. The nanopatterned HMM has a grating period of $a=200$ nm and width of $d=40$ nm. **c,d**, Purcell factor (**c**) and radiative enhancement (**d**) corresponding to the dashed lines in **a** and **b** are replotted for comparison. **e**, Purcell factor as a function of emission wavelength for isotropic dipoles at locations indicated in **a**. **f**, Radiative enhancement as a function of emission wavelength for isotropic dipoles at locations indicated in **b**.

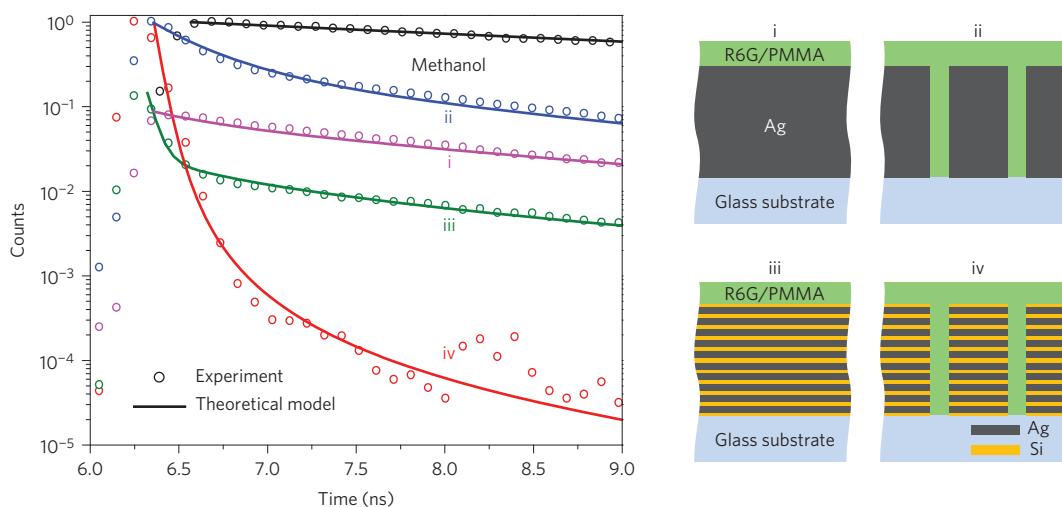


Figure 4 | Experimental measurements and theoretical fit of time-resolved fluorescence for dye molecules on different samples. Time-resolved fluorescence measurements for R6G on the nanopatterned Ag-Si HMM (iv, red circles), Ag grating (ii, blue circles) and in methanol solutions (black circles) after being normalized to the maximum of individual curves observed at an emission wavelength of 560 nm. Grating period, 200 nm. Data for a uniform Ag-Si HMM (iii, green circles) and a Ag single layer (i, purple circles) are divided by the same normalization factor as used for the nanopatterned Ag-Si HMM and Ag grating, respectively. Corresponding theoretical fit curves in solid lines explain well the spontaneous emission behaviour in the time domain. Right: schematics of the analysed samples.

from contributions from both enhanced radiative emission and the larger excitation electric field intensity. Smaller grating periods better match and outcouple high-wavevector plasmonic modes, resulting in a simultaneous enhancement of both the Purcell factor and fluorescent intensity. Nevertheless, optimized designs

that compensate multiple mismatched wavevectors may further help outcouple more high-wavevector modes.

To understand Purcell enhancement and the outcoupling effect in the nanopatterned multilayer HMMs, we adopted a dynamic Lorentzian model²⁶ to explain the spontaneous emission behaviour

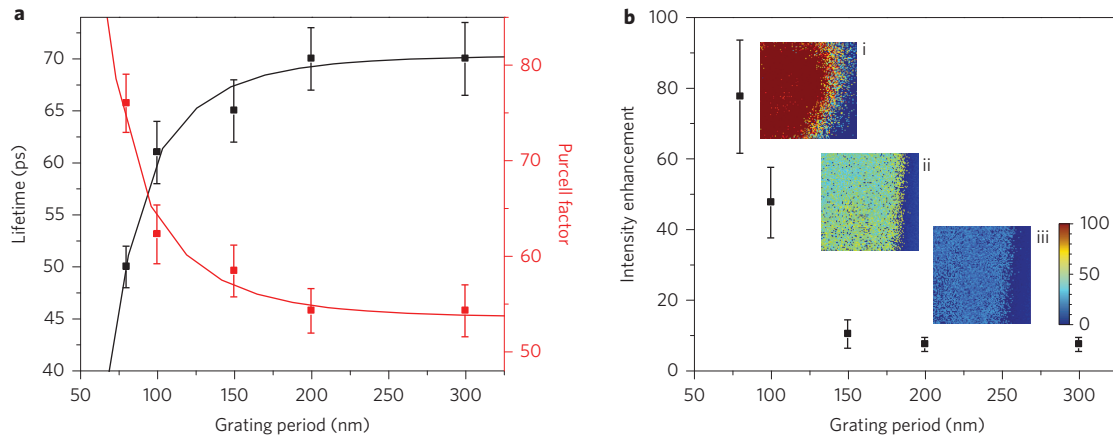


Figure 5 | Experimental demonstration of the geometrical dependence of Purcell and fluorescence intensity enhancement on nanopatterned multilayer HMMs. **a**, Lifetime (black) measured at the maximum decay rate of time-resolved fluorescence, and the corresponding Purcell factor (red) for R6G on the nanopatterned Ag-Si HMM with different grating periods. Solid lines are a guide to the eye. **b**, Fluorescence intensity enhancement for R6G on the nanopatterned Ag-Si HMM with different grating periods. Inset: optical images of the fluorescence intensity accumulated over 100 frames (grating periods: (i) $a = 80$ nm; (ii) $a = 100$ nm; (iii) $a = 200$ nm). Error bars represent the fluctuations in fluorescence photo-counts.

in the time domain (Supplementary Section 3). Because Purcell enhancement depends on dipole-substrate distance, the time-resolved fluorescence measures an averaged effect from molecules distributed within the PMMA layer thickness. The theoretical model takes this into account by averaging the time response of the dipoles at different spatial locations, whereas the outcoupling effect of the nanopatterns is taken into account by introducing an effective outcoupling coefficient into the model (Supplementary equation (10)). The theoretical fit based on this model is given as solid lines in Fig. 4, which agrees well with experimental measurements (see Supplementary Section 3 for the fitting procedure). The model not only predicts the change in spontaneous emission rates at different times determined by the interaction strength of molecules with the substrate, but also explains the outcoupling mechanism that helps improve the radiative emission, for better identification of the Purcell enhancement of the system.

In conclusion, we have shown that the spontaneous emission rate of a dye molecule embedded in a polymeric matrix can be greatly enhanced by nanostructuring HMMs composed of alternating multilayers of Ag and Si. In nanopatterned HMMs, non-radiative plasmonic modes are outcoupled, resulting in a 76-fold enhancement in Purcell factor and an 80-fold enhancement in emission intensity compared to HMMs without nanostructuring. In addition, theoretical calculations show that these enhancements can be tuned to a desired wavelength across the visible spectrum by changing the metallic filling ratio in the HMMs. Further improvements can be obtained by optimizing the distribution of dipole emitters and the design of the nanostructure geometry. Engineering plasmonic DOS using outcoupling nanostructures in multilayer HMMs can provide desired tunability of Purcell factor enhancement for light emission, with both high speed and high radiative intensity at broadband operational frequencies, for applications in biosensing, surface-enhanced Raman spectroscopy and light-emitting devices.

Methods

Fabrication of nanopatterned multilayer HMMs. Ag-Si multilayers, composed of 15 pairs of 10 nm Ag and 10 nm Si layers with a capping Si layer of 5 nm, were prepared by alternately d.c. magnetron sputtering Si and Ag layers onto glass substrates at room temperature. Sputtering rates for Ag and Si at 50 W ($\sim 2.5 \text{ W cm}^{-2}$) were 1.6 \AA s^{-1} and 0.16 \AA s^{-1} , respectively, as determined by low-angle X-ray reflectivity measurements of calibration sample film thicknesses. The 5 nm capping layer helps prevent Ag oxidation as well as rapid quenching of emitters in the vicinity of the metal surface. The base pressure of the chamber was 5×10^{-8} torr and the Ar pressure was fixed at 2.0 mtorr. Nanoscale trenches were inscribed into the multilayers by focused ion beam (FIB) milling with

different periods to form grating nanostructures. The Ga ion implantation effect introduced during the FIB milling process was not observed in our experiments. The fluorescence R6G dye molecules mixed in PMMA were spin-coated onto the uniform and nanopatterned surface of the multilayers to a thickness of 80 nm. A flat PMMA top surface was formed (Supplementary Fig. 5).

Measurements of time-resolved photoluminescence. The lifetime of the R6G dye molecules on various samples was measured by time-resolved photoluminescence in a two-photon microscope system²⁷. A Ti:sapphire laser system (Spectra-Physics Mai Tai) with a pulse width of less than 100 fs and a repetition rate of 80 MHz was applied to excite R6G with an excitation wavelength of 800 nm. A dichroic filter (700 nm) was used to block the laser light from detection. Through an emission filter at 560 nm with a bandwidth of 15 nm, the fluorescence signal was collected by a $\times 20$ objective (numerical aperture = 0.4) before being recorded by a Hamamatsu photomultiplier tube.

Received 7 March 2013; accepted 15 November 2013;
published online 6 January 2014

References

- Barnes, W. L., Dereux, A. & Ebbesen, T. W. Surface plasmon subwavelength optics. *Nature* **424**, 824–830 (2003).
- Schuller, J. A. *et al.* Plasmonics for extreme light concentration and manipulation. *Nature Mater.* **9**, 193–204 (2010).
- Shimizu, K. T., Woo, W. K., Fisher, B. R., Eisler, H. J. & Bawendi, M. G. Surface-enhanced emission from single semiconductor nanocrystals. *Phys. Rev. Lett.* **89**, 117401 (2002).
- Anger, P., Bharadwaj, P. & Novotny, L. Enhancement and quenching of single-molecule fluorescence. *Phys. Rev. Lett.* **96**, 113002 (2006).
- Okamoto, K. *et al.* Surface-plasmon-enhanced light emitters based on InGaN quantum wells. *Nature Mater.* **3**, 601–605 (2004).
- Cho, C.-H. *et al.* Tailoring hot-exciton emission and lifetimes in semiconducting nanowires via whispering-gallery nanocavity plasmons. *Nature Mater.* **10**, 669–675 (2011).
- Purcell, E. M. Spontaneous emission probabilities at radio frequencies. *Phys. Rev.* **69**, 681 (1946).
- Lakowicz, J. R. Radiative decay engineering 5: metal-enhanced fluorescence and plasmon emission. *Anal. Biochem.* **337**, 171–194 (2005).
- Fort, E. & Gresillon, S. Surface enhanced fluorescence. *J. Phys. D* **41**, 013001 (2008).
- Ford, G. W. & Weber, W. H. Electromagnetic interactions of molecules with metal surfaces. *Phys. Rep.* **113**, 195–287 (1984).
- Barnes, W. L. Fluorescence near interfaces: the role of photonic mode density. *J. Mod. Opt.* **45**, 661–699 (1998).
- Krishnamoorthy, H. N. S., Jacob, Z., Narimanov, E., Kretzschmar, I. & Menon, V. M. Topological transitions in metamaterials. *Science* **336**, 205–209 (2012).
- Jacob, Z. *et al.* Engineering photonic density of states using metamaterials. *Appl. Phys. B* **100**, 215–218 (2010).
- Ni, X. *et al.* Effect of metallic and hyperbolic metamaterial surfaces on electric and magnetic dipole emission transitions. *Appl. Phys. B* **103**, 553–558 (2011).

15. Tumkur, T. *et al.* Control of spontaneous emission in a volume of functionalized hyperbolic metamaterial. *Appl. Phys. Lett.* **99**, 151115 (2011).
16. Kim, J. *et al.* Improving the radiative decay rate for dye molecules with hyperbolic metamaterials. *Opt. Express* **20**, 8100–8116 (2012).
17. Liu, Z., Lee, H., Xiong, Y., Sun, C. & Zhang, X. Far-field optical hyperlens magnifying sub-diffraction-limited objects. *Science* **315**, 1686–1701 (2007).
18. Zhang, X. & Liu, Z. Superlenses to overcome the diffraction limit. *Nature Mater.* **7**, 435–441 (2008).
19. Zheludev, N. I. & Kivshar, Y. S. From metamaterials to metadevices. *Nature Mater.* **11**, 917–924 (2012).
20. Lu, D. & Liu, Z. Hyperlenses and metalenses for far-field super-resolution imaging. *Nature Commun.* **3**, 1205 (2012).
21. Cortes, C. L., Newman, W., Molesky, S. & Jacob, Z. Quantum nanophotonics using hyperbolic metamaterials. *J. Opt.* **14**, 063001 (2012).
22. Jacob, Z. & Shalae, V. M. Plasmonics goes quantum. *Science* **334**, 463–464 (2011).
23. Yang, X., Yao, J., Rho, J., Yin, X. & Zhang, X. Experimental realization of three-dimensional indefinite cavities at the nanoscale with anomalous scaling laws. *Nature Photon.* **6**, 450–454 (2012).
24. Cui, Y. *et al.* Ultrabroadband light absorption by a sawtooth anisotropic metamaterial slab. *Nano Lett.* **12**, 1443–1447 (2012).
25. Selinger, K. A., Falnes, J. & Sikkeland, T. Fluorescence lifetime studies of Rhodamin 6G in methanol. *J. Phys. Chem.* **81**, 1960–1963 (1977).
26. Wang, J., Chabanov, A. A., Lu, D. Y., Zhang, Z. Q. & Genack, A. Z. Dynamics of mesoscopic fluctuations of localized waves. *Phys. Rev. B* **81**, 241101 (2010).
27. Stringari, C. *et al.* Phasor approach to fluorescence lifetime microscopy distinguishes different metabolic states of germ cells in a live tissue. *Proc. Natl Acad. Sci. USA* **108**, 13582–13587 (2011).

Acknowledgements

The authors acknowledge financial support from an Office of Naval Research (ONR) Young Investigator Award (no. N00014-13-1-0535), the National Science Foundation–Electrical, Communications and Cyber Systems (NSF-ECCS) (grant no. 0969405) and the National Science Foundation–Civil, Mechanical and Manufacturing Innovation (NSF-CMMI) (grant no. 1120795). The authors thank P. Zhang for help with STEM characterization and M. Digman, E. Gratton, L. Feng, H. Chen and Y. Liu for assistance during various phases of simulations and experiments. The time-resolved photoluminescence measurements were carried out at the Laboratory for Fluorescence Dynamics (LFD) at the University of California, Irvine (UCI). The LFD is supported jointly by the National Center for Research Resources (5P41RR003155-27), the National Institute of General Medical Sciences of the National Institutes of Health (8P41GM103540) and UCI.

Author contributions

Z.L. conceived the concept. D.L. performed numerical modelling and simulations, in detail. J.J.K. and D.L. fabricated the samples. D.L. performed the optical experiments and prepared all the figures. D.L., Z.L. and J.J.K. wrote the manuscript. All authors discussed the results and commented on the manuscript. Z.L. supervised the project.

Additional information

Supplementary information is available in the [online version](#) of the paper. Reprints and permissions information is available online at www.nature.com/reprints. Correspondence and requests for materials should be addressed to Z.L.

Competing financial interests

The authors declare no competing financial interests.